ELSEVIER

Carbohydrate Research 286 (1996) 17–39

CARBOHYDRATE RESEARCH

Binding properties of carbohydrate sulfamates based on ab initio 6-31 + G** calculations on *N*-methyl and *N*-ethyl sulfamate anions

Dennis M. Whitfield [a,*], Doriano Lamba [b], Ting-Hua Tang [c,1,d], Imre G. Csizmadia [c]

[a] *National Research Council of Canada, Ottawa, Ontario K1A 0R6, Canada*
[b] *Istituto di Strutturistica Chimica Giordano Giacomello, Area della Ricerca di Roma, CNR CP No. 10, I-00016 Monterotondo Stazione, Rome, Italy*
[c] *Department of Chemistry, University of Toronto, Toronto, Ontario M5S 1A1, Canada*
[d] *Department of Chemistry, Tianjin Normal University, Tianjin 300074, People's Republic of China*

Received 18 September 1995; accepted 21 January 1996

Abstract

2-Deoxy-2-sulfoamino-D-glucopyranoside anions are uniquely found in heparin-like biopolymers. Due to the bioactivities of these biopolymers, there is considerable interest in developing heparin mimetics as potential therapeutic agents. The chemical bonding of such anions is analyzed by topological analysis of the electron-density distribution based on ab initio 6-31 + G** calculations. The results support an amine-like pyramidal geometry for nitrogen with a well-defined maximum in the Laplacian of the charge density consistent with a lone pair of electrons. Water complexes of the *N*-methyl sulfamate anions give insight into binding motifs, including bifurcated hydrogen-bonded systems and hydrogen-bond properties for the sulfoamino nitrogen. Finally, by systematic variation of the structural parameters of these *N*-alkyl sulfamate anions, MM+ parameters for this group in sugars were determined. The structural properties calculated by molecular modeling agree well with the ab initio results and with three crystal structures of sodium 2-deoxy-2-sulfoamino-α-D-glucopyranose derivatives. © 1996 Elsevier Science Ltd.

Keywords: Heparin; D-Glucopyranoside, 2-deoxy-2-sulfoamino-; Sulfamate, *N*-methyl-; Sulfamate, *N*-ethyl-; Ab initio calculations

* Corresponding author.
[1] Also corresponding author. Current address: Department of Chemistry, McMaster University, Hamilton, Ontario, Canada L8S 4M1.

PII S0008-6215(96)00032-8

1. Introduction

The sulfamate anion is found in Nature only in higher mammals as part of the biopolymers, heparin and heparan sulfate [1]. This unusual functional group ($R–NH–SO_3^-$) has been shown to be essential for the following: (*i*) the in vivo bioactivity of heparin as an antithrombotic agent [2], (*ii*) heparin binding to the basic fibroblast growth factor [3], and (*iii*) heparin binding to the herpes simplex virus [4]. In general, numerous other activities of heparin also depend on the presence of acidic sulfate groups (for examples, see ref. [5]). These bioactivities have prompted the developments of mimetics as potential therapeutic agents. This paper describes some theoretical studies aimed at clarifying the chemical properties of sulfamates that could aid in the development of such mimetics.

The first section describes the results of ab initio 6-31 + G** calculations aimed at understanding the nature of the chemical bonding in sulfamate anions. Previous work carried out by us focused on the properties of sulfate esters [6]. We have adopted the same procedures to study the sulfamate groups so that meaningful comparisons can be made between the two functionalities. The nitrogen of the sulfamate group has the additional complexity (compared to sulfate esters) of being potentially chiral if its substituents are pyramidal (amine-like) [7]. If the substituents are planar (amide-like), then the nitrogen is not a chiral center. Besides the geometry at the nitrogen atoms, another characteristic of amine nitrogens is the presence of a well-defined lone electron pair, indicating sp^3 hybridization at nitrogen. Amide nitrogens have sp^2 hybridization, and the extra electrons are delocalized into adjacent chemical bonds. In this work we use Bader's theory of atoms in molecules (AIM) to describe the bonding and to distinguish between sp^2 and sp^3 hybridization [8].

Ab initio calculations in general and the AIM theory in particular are good methods to study hydrogen-bonding and other noncovalent interactions as well as covalent interactions. Since the long-term objective of this work is to help elucidate the binding properties of sulfamate groups, we decided to consider each of the oxygens bound to sulfur to be distinctly different. As shown in Fig. 1, staggered conformations have one sulfur-bound oxygen *anti* to the carbon–nitrogen bond, and each of the *gauche* (to carbon) oxygens are either *anti* or *gauche* to the nitrogen–hydrogen bond. Thus, specific interactions with any of these oxygens such as hydrogen-bonding or metal

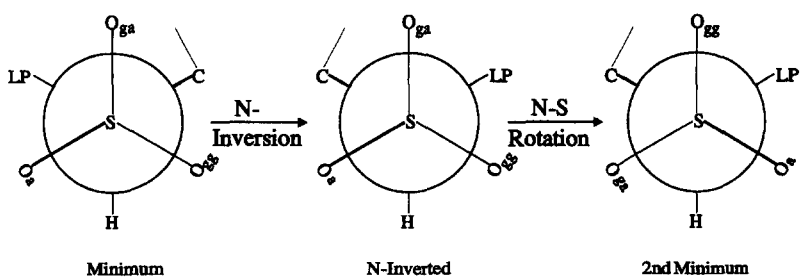

Fig. 1. Newman projections about the S–N bond for *N*-alkyl sulfamates. The definitions for O_a, O_{gg}, and O_{ga} refer to the minimum structure on the left and are only used as labels for the other two isomers.

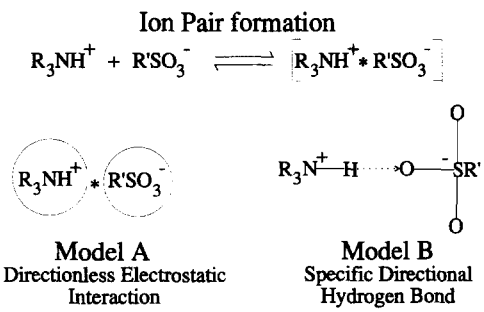

Fig. 2. Two models for ion-pair formation between protonated basic amino acid side chains and anionic sugar sulfate groups.

coordination will put the bonding partner in a different relationship with the nitrogen substituents. This contrasts with the sulfate esters where the two *gauche* (to carbon) oxygens are nearly equivalent. Also shown in Fig. 1 is the epimer at nitrogen. This leads to a higher-energy rotamer that must relax by rotation. Water complexes of *N*-methyl sulfamate **1** were studied by ab initio methods as prototypes of noncovalent interactions of sulfamate anions.

The second section describes some preliminary results using molecular modeling to analyze the nature of chemical bonding of sulfamates in heparin-like molecules. Heparins are frequently found in vivo, bound to protein receptors. In most cases atomic-level resolution of this bonding has not been obtained. Molecular-level resolution of protein–heparin interactions is derived from binding studies where the amino acids of the protein [9] or peptide [10] are varied, or variously derivitized heparin fragments [11] are used [12]. Such studies have unambiguously shown the importance of basic amino acids for binding such as lysine, arginine [13] and histamine [14]. It is readily deduced that the positively charged functional groups of these amino acid side chains can interact through nonspecific electrostatic interactions with the sulfate groups in heparin. However, it is not known if directionally specific hydrogen bonds are formed in such interactions. Fig. 2 schematically shows these two models of ion-pair formation. In biological systems such interactions will always operate in competition with water-binding to both the amino acids and the sugars. Thus, it is necessary to understand both water-binding and the interactions of amino acids with charged molecules.

2. Computational methods

Molecular mechanics.—All calculations used the version of MM+ [15] supplied with the Hyperchem v. 4 PC-based package of programs (Hypercube, Waterloo, Ontario, Canada) that includes parameters published up to 1990. Our new parameters are tabulated in Table 1 and were entered into the program by modifying the appropriate parameter files. All parameters were determined by nonlinear least-squares fitting of the ab initio data to the following equations: $E = k_s(r - r_0)^2$ for bond length r, $E = k_\theta(\theta - \theta_0)^2$ for bond angle θ, and $E = V_1/2(1 + \cos\omega) + V_2/2(1 - \cos 2\omega) + V_3/2(1 +$

Table 1
Calculated parameters for sulfamates for use in MM+ calculations

	Bond length r_0 (Å)	k_s (mdyn Å^{-1})	Bond dipole (mdyn)	r^2
S–O_a	1.453	10.006	−3.0	0.995
S–O_{gg}	1.452	9.495	−3.0	0.995
S–O_{ga}	1.460	10.044	−3.0	0.996
S–N	1.692	4.117	−1.0	0.997
N–H_s	1.003	7.952	−1.31	0.995
C–N	1.451	5.750		0.997
	Bond angle θ_0 (°)	k_θ (mdyn Å rad^{-2})		r^2
O_{gg}–S–N	106.54	1.960		0.998
O_{ga}–S–N	104.56	1.920		0.997
O_a–S–N	102.91	1.953		0.997
O_{ga}–S–O_{gg}	113.40	2.426		0.999
O_{gg}–S–O_a	113.75	2.226		0.999
O_{ga}–S–O_a	115.76	2.162		0.999
S–N–C	115.98	1.107		0.994
S–N–H_s	106.99	0.754		0.999
	Torsion angles (°)			r^2
	V_1	V_2	V_3	
CN–SO_a	0.020	0.046	3.226	0.909
HC–NS	−0.012	−0.021	2.265	0.995
CC–NS	2.918	0.287	−0.147	0.981

$\cos 3\omega$) for bond torsion angle ω using the statistics program InPlot (GraphPad, San Diego, CA). Since the raw ab initio is not presented, the parameters are given to three decimal points to allow the reader to extract the data (most values at the minima are given in Fig. 3). All other parameters (e.g., van der Waals parameters) were the same as in the existing Hyperchem MM+ parameters. Minimizations used either the normal Newton–Raphson method or the Fletcher–Reeves conjugate gradient method. The D-glucosamine structure was taken from the library of monosaccharide structures (Chemplus–Hypercube). Minimization (MM+) was carried out after the addition of

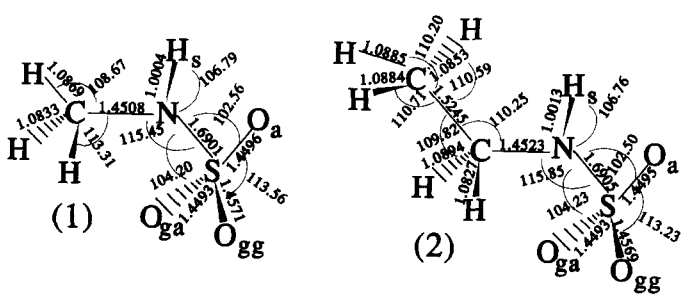

Fig. 3. SCF 6-31+G** optimized geometries for **1** and **2** with selected bond lengths and bond angles indicated.

each substituent, methyl, *O*- or *N*-sulfo. For methyl **1**, ethyl **2**, isopropyl **7** and glucosamine sulfamates **8–10**, minimization was to a gradient of 0.00001 kcal $Å^{-1} mol^{-1}$. Subsequently the conformation about the O–S–N–C bond for *N*-methyl **1** and the S–N–C–C bond for the remaining molecules **7–10** was tested using the conformational searching algorithm of ref. [16] as implemented in Chemplus, an add-on program to Hyperchem. Comparisons to the ab initio structures were made by using the RMSD (root-mean-square deviation of coordinates) routine in Chemplus by either importing the crystal coordinates after conversion to Cartesian coordinates or by importing the ab initio output files as *Z*-matrices.

The present version of MM+ does not contain parameters for sodium cations nor does the AM1 routine allow for charge calculations with sodium. In order to investigate the effect of the counter-ion, a very tentative exploration was made using the charges calculated for Li^+ (parameters in AM1) and the van der Waals constants from the AMBER program (1.60 Å, 0.05) provided with Hyperchem. The resulting minimized structures were then recalculated (Li^+ exchanged for Na^+) for charges using AM1, and then reminimized by MM+.

AM1 semiempirical point charges.—All calculations used the version of AM1 [17] supplied with Hyperchem. Structures were first built and minimized using molecular mechanics (ion–dipole option using default values, cf. Table 1 and ref. [18]). Single-point AM1 calculations were then performed on this geometry, and the resultant point charges (Mulliken) were then used in the MM+ calculation. A second AM1 single-point calculation was made to redetermine the point charges at the new minimum geometry, and then a final MM+ calculation was made. Selected computations using the ab initio point charges (Mulliken) or Bader's AIM atomic charges were performed by manually editing the Hyperchem v. 4 input files. For conformational searches the charges of the initial input structure were used for all conformations.

Ab initio MO calculations.—All calculations were performed on either an HP-755 or an Apollo DN 10000 minicomputer using GAUSSIAN 88 [19] and GAUSSIAN 92 [20] programs. The 6-31 + G** basis set was chosen for all ab initio studies. The 6-31 + G** basis set was derived by taking a standard split-valence basis 6-31G [21] and adding *d*-orbitals as the polarization functions and a simple diffuse *sp*-shell for all heavy atoms, and *p*-orbitals as polarization functions for hydrogen atoms. It was found that the diffuse functions have a significant effect on the energies and geometries of anions because of the improved description of long-range behaviour of molecular orbitals, particularly those that are describing the lone electron pairs. For all systems, full gradient geometry optimizations were carried out, and the total energies and Mulliken populations [22] were determined.

The topological analysis of electron-density distribution in the theory of atoms in molecules (AIM) [23] has been discussed elsewhere [6,24], and only a few key points will be repeated here. This topological analysis is based on the gradient vector field of the electronic density $\nabla\rho(\boldsymbol{r})$, and on the Laplacian of electronic density $\nabla^2\rho(\boldsymbol{r})$. An atom in a molecule is defined as a region of real three-dimensional space bound by a zero-flux surface of the gradient vector field of $\rho(\boldsymbol{r})$. Critical points in $\rho(\boldsymbol{r})$ are classified by the three eigenvalues λ_i ($i = 1,2$, and 3) of the Hessian matrix ($H_{ij} = \partial^2\rho(\boldsymbol{r})/\partial x_i\,\partial x_j$). In general there are four types of critical points (3, −1), (3, +1), (3, −3), and (3, +3) that

can be characterized by two numbers. The first number labels their rank (number of nonzero eigenvalues), and the second number is the signature (excess number of positive over negative eigenvalues). In the present study only the first three critical points occur. A (3, −3) critical point is a local maximum that occurs generally at the nuclear position. Secondly, a (3, −1) critical point, at which $\rho(\boldsymbol{r})$ has two negative curvatures and one positive curvature, actually is a bond critical point (BCP). In other words, two interacting atoms in a molecule form, at the position $\boldsymbol{r}_b$, a single BCP in the electron density, where $\nabla\rho(\boldsymbol{r}) = 0$. The point $\boldsymbol{r}_b$ represents a minimum in charge density along the bond and a maximum in charge density perpendicular to the bond. The pair of gradient paths, which originate at a BCP and terminate at neighbouring nuclei, define a line, called a bond path, through the electron-density distribution along which $\rho(\boldsymbol{r})$ is a maximum with respect to any lateral displacement. The necessary condition for two atoms to be bonded to one another is that their nuclei be linked by a bond path. The network of bond paths for a molecule in a given nuclear configuration **X** defines the molecular graph. Such a topological graph usually corresponds to the commonly drawn chemical-bond network. The electron density, $\rho(\boldsymbol{r}_b)$, at the BCP is related to the bond strength and bond order, and it is found to be significantly larger for a double bond than for a corresponding single bond. The second derivatives of ρ at the BCP (λ_1, λ_2, and λ_3) indicate how rapidly ρ changes on moving away from the BCP and represents the curvatures of charge density along different directions. For a normal single bond, such as the C–C bond in ethane, the two negative curvatures (λ_1 and λ_2), which are perpendicular to the bond line, are equal. However, if there is a double bond, one curvature (in the direction of the π-bond) will be much smaller than the other. This difference may be described by the ellipticity of the bond, which is defined as $\epsilon = \lambda_1/\lambda_2 - 1$. For symmetrical triple C ≡ C bonds, since $\lambda_1 \approx \lambda_2$, ϵ is equal to or close to zero. In practice, the trace or the sum of the second partial derivative values, $\nabla^2\rho(\boldsymbol{r}_b) = \sum_{j=1,3}\partial^2\rho(\boldsymbol{r})/\partial x_j^2$, at the BCP is negative for a covalent interaction, and the condition $\nabla^2\rho(\boldsymbol{r}_b) > 0$ indicates an interaction between closed-shell systems (including ionic interactions). As a sufficient condition [25], one can determine the sign of the local energy density ($H_b = G_b + V_b$, i.e., the local energy density is the sum of the kinetic- and potential-energy densities). The sign of H_b varies as follows: $H_b \equiv H(\boldsymbol{r}_b) < 0$ for covalent bonds; $H_b \equiv H(\boldsymbol{r}_b) > 0$ for ionic bonds. Thirdly, a (3, +1) critical point, at which $\rho(\boldsymbol{r})$ has one negative curvature and two positive curvatures, is equally a RCP. The existence of a RCP, at which the density $\rho(\boldsymbol{r})$ is smaller than that of all surrounding BCPs, indicates that the molecule contains a ring structure.

Starting at a BCP, paths for which the electron density decreases most rapidly are developed in all directions normal to the bond. The set of such paths defines a zero-flux surface separating a pair of atoms. A set of those surfaces (one per bond) will partition a molecule into unique atomic regions (basins) for which the hypervirial theorem is satisfied. Numerical integration of the electron density within such a region yields the population assigned to the given atom [26]. This is called the AIM atomic charge.

The Laplacian of the electron density, the quantity at any point $\nabla^2\rho(\boldsymbol{r})$, determines the space wherein the electron density is locally concentrated or depleted. From the definition of a second derivative, one finds that $\rho(\boldsymbol{r})$ is greater than the average of its values over an infinitesimal sphere centered on $\boldsymbol{r}$ when $\nabla^2\rho(\boldsymbol{r}) < 0$, and $\rho(\boldsymbol{r})$ is less

Table 2
N-methyl sulfamate **1** and *N*-ethyl sulfamate **2**: Calculated harmonic vibrational frequencies at the 6-31 + G** level [a]

Mode	**1**			**2**	
	Frequencies (cm^{-1})	Assignments [b]	IR intensities [c]	Frequencies (cm^{-1})	IR intensities [c]
$\upsilon 1$	101.3	SO_3 t	1.75	72.7	1.62
$\upsilon 2$	199.2	CH_3 t	0.27	98.9	1.05
$\upsilon 3$	248.3	CNS, NSO b	6.57	182.0	3.37
$\upsilon 4$	415.8	NSO b as	7.52	274.3	0.64
$\upsilon 5$	448.0	NSO b s	8.21	353.6	4.35
$\upsilon 6$	578.9	CNS, NSO b	46.90	408.9	6.78
$\upsilon 7$	592.3	O = S = O b as	10.21	439.8	5.29
$\upsilon 8$	650.2	O = S = O b s	44.31	581.4	43.58
$\upsilon 9$	782.7	N–H b	257.81	598.9	17.21
$\upsilon 10$	882.2	N–S st	70.73	678.1	95.30
$\upsilon 11$	1114.2	C–N st	196.43	794.7	184.74
$\upsilon 12$	1168.9	S = O st s	43.20	860.4	33.98
$\upsilon 13$	1246.2	NCH b	21.39	921.6	49.26
$\upsilon 14$	1256.2	NCH b	6.34	998.3	18.15
$\upsilon 15$	1306.1	S = O st as	460.6	1113.5	225.69
$\upsilon 16$	1340.9	S = O st as	399.32	1156.9	41.07
$\upsilon 17$	1559.1	HNC, CNS b	40.66	1236.1	8.51
$\upsilon 18$	1576.8	CH_2, NCH b	24.06	1262.3	28.07
$\upsilon 19$	1614.4	CH_3 b	0.68	1306.8	446.69
$\upsilon 20$	1644.9	CH_3 b	8.87	1340.4	382.84
$\upsilon 21$	3158.8	CH_3 st s	102.88	1400.8	24.38
$\upsilon 22$	3206.4	CH_3 st as	75.45	1493.8	1.39
$\upsilon 23$	3275.1	CH_3 st as	24.59	1534.1	2.48
$\upsilon 24$	3793.0	(N–H st)	7.92	1582.3	78.13
$\upsilon 25$				1611.5	12.11
$\upsilon 26$				1619.6	0.94
$\upsilon 27$				1651.4	1.77
$\upsilon 28$				3153.0	42.27
$\upsilon 29$				3164.1	69.16
$\upsilon 30$				3203.3	67.97
$\upsilon 31$				3240.1	51.59
$\upsilon 32$				3262.4	41.88
$\upsilon 33$				3781.4	6.57

[a] The zero-point vibrational energy (ZPVE) (**1**) 45.97 kcal mol^{-1} and (**2**) 64.87 kcal mol^{-1}.
[b] Assignments from ref. [29]: st (stretch), s (symmetric), as (antisymmetric), b bend, t torsion.
[c] In KM mol^{-1}.

than average when $\nabla^2\rho(\boldsymbol{r}) > 0$. The outer quantum shell of an atom is divided into an inner region over which $\nabla^2\rho(\boldsymbol{r}) < 0$ and an outer one over which $\nabla^2\rho(\boldsymbol{r}) > 0$. The portion of the shell over which $\nabla^2\rho(\boldsymbol{r}) < 0$ is called the valence shell charge concentration (VSCC). Thus a local maximum (or minimum) in $-\nabla^2\rho(\boldsymbol{r})$ (within the VSCC) of a bonded atom signifies a local concentration (or depletion) of electron density. The numbers, locations and relative sizes of the bonded and the nonbonded concentration of electron density in the valence shell of a bonded atom as determined by the Laplacian of

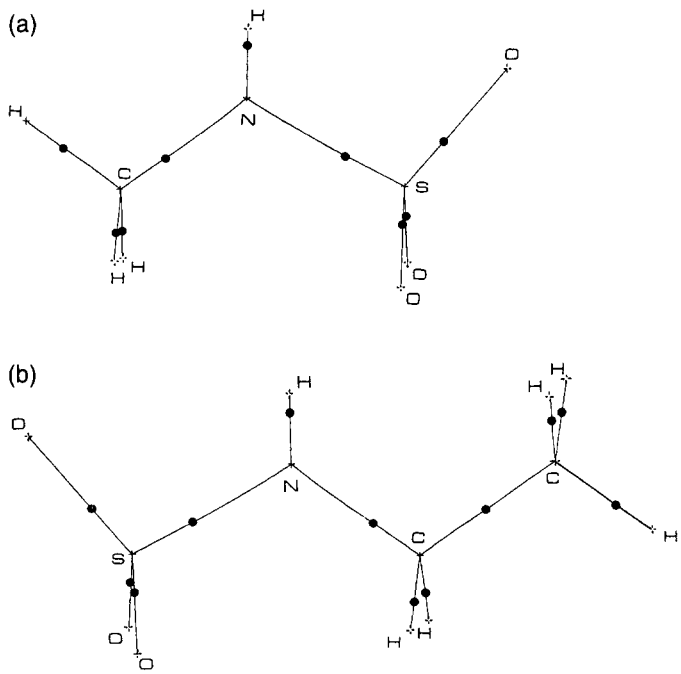

Fig. 4. Molecular graphs for (a) **1** and (b) **2** in their 6-31+G** optimized geometries (3, −3) nuclear positions, +, and (3, −1) BCPs, ●.

$\rho(\boldsymbol{r})$ are found to be in generally good agreement with the corresponding properties that are ascribed to bonded and nonbonded pairs in Gillespie's valence shell electron pair repulsion (VSEPR) model of molecular geometry [27]. The AMPAC program was employed for the electron-density topological analysis, using the electron density obtained from the 6-31 + G** calculations. [2]

3. Results and discussion

(a) Chemical bonding from ab initio calculations.—Fig. 3 shows the important structural parameters for *N*-methyl **1** and *N*-ethyl sulfamate **2** anions derived from ab initio calculations at the 6-31 + G** level in their minimum-energy conformations. The 6-31 + G** calculation level was found to be adequate for studying sulfate ester anions [6,28]. Table 2 presents the unscaled vibrational frequencies derived from these calculations. The assignments for *N*-methyl sulfamate anion follow from ref. [29]. In both molecules the calculated structural parameters for the O–S and N–S bonds are very similar.

[2] Available from Professor R.F.W. Bader's laboratory, McMaster University, Hamilton, Ontario, Canada L8S 4M1.

Table 3
N-methyl sulfamate **1** and *N*-ethyl sulfamate **2**: The topological properties of electron-density distributions at the BCPs from 6-31 + G** calculations

Bond	ρ_b (au)	$\nabla^2\rho_b$ (au)	ϵ	H_b (Hartree Å^{-3})
1 C–N	0.2753	−0.9054	0.0216	−2.6637
1 N–S	0.2241	−0.1717	0.0515	−1.9183
1 S–O_a	0.2969	1.3384	0.0372	−2.2708
1 S–O_{ga}	0.2971	1.3436	0.0411	−2.2721
1 S–O_{gg}	0.2932	1.2775	0.0473	−2.2458
1 C–H_a	0.2878	−1.0707	0.0376	−2.1222
1 C–H_g	0.2910	−1.0956	0.0349	−2.1391
1 C–$H_{g'}$	0.2957	−1.1424	0.0301	−2.2073
1 N–H	0.3606	−1.9589	0.0534	−3.7171
2 C–C	0.2587	−0.6996	0.0356	−1.5226
2 C–N	0.2750	−0.8960	0.0307	−2.6833
2 N–S	0.2235	−0.1683	0.0507	−1.9102
2 S–O_a	0.2970	1.3392	0.0372	−2.2714
2 S–O_{ga}	0.2971	1.3430	0.0408	−2.2721
2 S–O_{gg}	0.2934	1.2793	0.0465	−2.2484
2 C-2–H_a	0.2831	−1.0262	0.0023	−2.0682
2 C-2–H_g	0.2828	−1.0255	0.0038	−2.0668
2 C-2–$H_{g'}$	0.2872	−1.0624	0.0020	−2.1094
2 C-1–H	0.2981	−1.1563	0.0246	−2.2302
2 C-1–H′	0.2924	−1.1009	0.0310	−2.1506
2 N–H	0.3595	−1.9491	0.0529	−3.7016

Molecular graphs for the equilibrium geometries of **1** and **2** at the 6-31 + G** level of theory are plotted in Fig. 4. The topological parameters derived from the electron-density distributions at the BCPs of **1** and **2** are listed in Table 3. As shown in the previous paper describing *O*-alkyl sulfates [6], all S–O bonds are covalent but highly polarized because of their positive values of $\nabla^2\rho_b$ and negative values of H_b. These bonds have an extensive S = O double-bond character because their ρ_b values (0.2932–0.2972 au) are similar to the typical S = O in Me_2SO (0.2723 au, cf. ref. [6]). However, two of the three oxygens, namely S–O_a and S–O_{ga}, have a slightly greater double-bond character than S–O_{gg}. Also, the $\nabla^2\rho_b$ value for the N–S bond of **1** is negative, but the corresponding value for the (C)O_s–S in *O*-methyl sulfate **5** is positive, and, for both, the H_b values are negative. It seems that the O_s–S is more polarized than the N–S bond in **1** or **2**.

More interestingly, the topological analysis of the electron-density distribution can be used to study whether the *N*-alkyl sulfamate compounds are amide-like or amine-like. This analysis can distinguish between amino- and amido-like nitrogens based on Laplacian concentrations. For an amino-like nitrogen, one nonbonded Laplacian concentration (corresponding to the lone pair of nitrogen in the VSEPR model) should exist around the nitrogen, and the angles between the nonbonded and bonded Laplacian concentrations are approximately tetrahedral. The contour maps of the Laplacian of ρ for the plane containing the N- and S-nuclei and the positions of the nonbonded

concentrations of **1** and **2** are shown in Fig. 5. Also shown for comparison in Fig. 5 are the contour maps of the Laplacian of ρ for the plane containing the C- and N-nuclei, as well as the position(s) of the Laplacian concentrations(s) around the nitrogen of

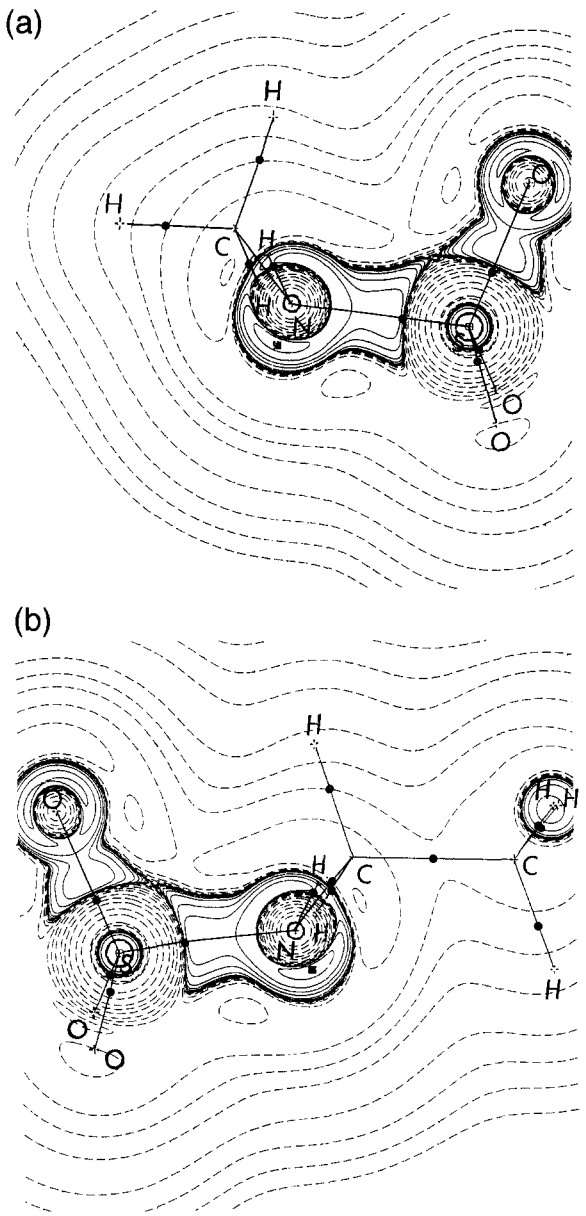

Fig. 5. Contour maps: in the N–S plane of the Laplacian of ρ for (a) **1** and (b) **2** and in the C–N plane for (c) **3** and (d) **4** in their SCF 6-31+G** optimized geometries. The nonbonded charge concentration on N is indicated by ■, and the (3, −3) nuclear positions, +, and (3, −1) BCPs, ●, are shown.

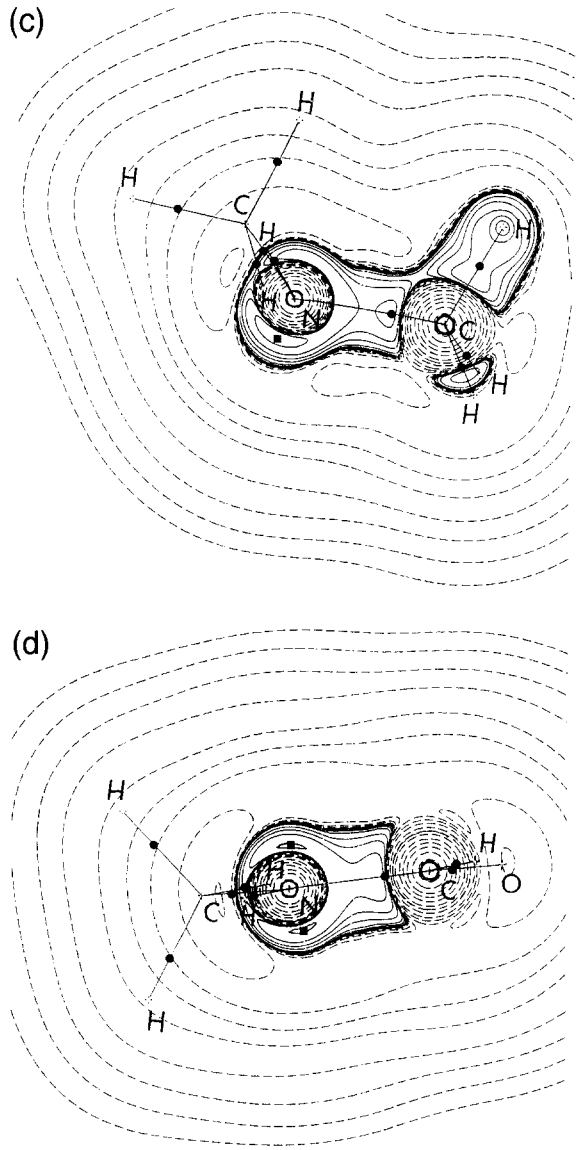

Fig. 5 (continued).

dimethylamine (**3**), which contains a typical amino nitrogen, and *N*-methylformamide (**4**), which contains a typical amido one. These last two calculations were at the same 6-31 + G** level of theory. The values of the Laplacian concentration, distances from the N-nuclei and the angles (n–N–b) between nonbonded and bonded concentrations for sulfamates **1** and **2** as well as **3** and **4** are listed in Table 4. For the nitrogen in **4** there are two Laplacian concentrations which represent the *p*-orbital of nitrogen that is perpendicular to the molecular plane in the MO model. Based on the criteria discussed

Table 4
The values and distances from the N-nucleus of nonbonded (n) Laplacian concentrations and the angles between nonbonded and bonded (b) Laplacian concentrations

Molecule	$\nabla^2\rho$(max) (au)	Distance (au)	n–N–b (°)
N-methyl sulfamate **1**	−3.2353	0.7328	108.13 (n–N–C)
			110.14 (n–N–H)
			104.12 (n–N–S)
N-ethyl sulfamate **2**	−3.2103	0.7333	107.72 (n–N–C)
			110.09 (n–N–H)
			104.09 (n–N–S)
Dimethylamine (**3**)	−3.3473	0.7312	114.34 (n–N–C)
			108.45 (n–N–H)
N-methyl formamide (**4**)	−2.1730	0.7532	90.00 (n–N–C)
			90.00 (n–N–CO)
	−2.1730	0.7532	90.00 (n–N–C)
			90.00 (n–N–CO)

above, the nitrogens in **1** and **2** are both clearly like **3** and hence amino-like. The barrier to N-inversion in *N*-alkyl alkylsulfonamides has been calculated to be about 2 kcal mol^{-1} [30]. Since the structure of the transition state for N-inversion of *N*-alkyl sulfamates is unknown, we did not attempt to estimate the barrier for N-inversion. This subject should be further investigated since the 2 kcal mol^{-1} for related molecules discussed above is lower than the rotation barriers discussed below (see section *(c)*).

(b) Water complexes studied by ab initio methods.—Similar to the water complexes of *O*-methyl sulfate anion [6], the complexes (**11a–d**) of one water and **1** were studied at the 6-31 + G** ab initio level of theory. Four structures were determined to be true minima by determining their Hessian eigenvalues. Molecular graphs of these complexes are plotted in Fig. 6. The important bond lengths and bond angles are tabulated in Table 5. A linear hydrogen-bonded system is shown in Fig. 6a with one water hydrogen-bonded to the O_a sulfamate oxygen. In Fig. 6b and c two water hydrogens bridge the O_{ga} and O_{gg}, as well as the O_a and O_{gg}, respectively, in bifurcated hydrogen-bonded systems. The existence of a (3, +1) RCP for these cyclic systems demonstrates the apparent stability of such systems (see Table 6). However, such four-center hydrogen bonds have only rarely been found experimentally [31]. The linear hydrogen bond shown in Fig. 6d is different with one water hydrogen-bonded to the sulfamate nitrogen. Water complexes (**11a–c**) are of similar stability, whereas **11d**, although of relatively high binding energy compared to neutral water complexes, is lower in predicted stability. The topological properties of the electron-density distributions at the BCPs of the water complexes **11a–d** are tabulated in Table 6. These values are typical of hydrogen-bonded systems. These complexes serve as models of hydrogen-bonding motifs for protein-sulfated carbohydrate interactions.

(c) Chemical bonding by molecular modeling.—One of the tools for elucidating the binding properties of heparin and related biopolymers is molecular modeling [32,33]. Such studies require parameters for all the functional groups [34,35]. Other groups have

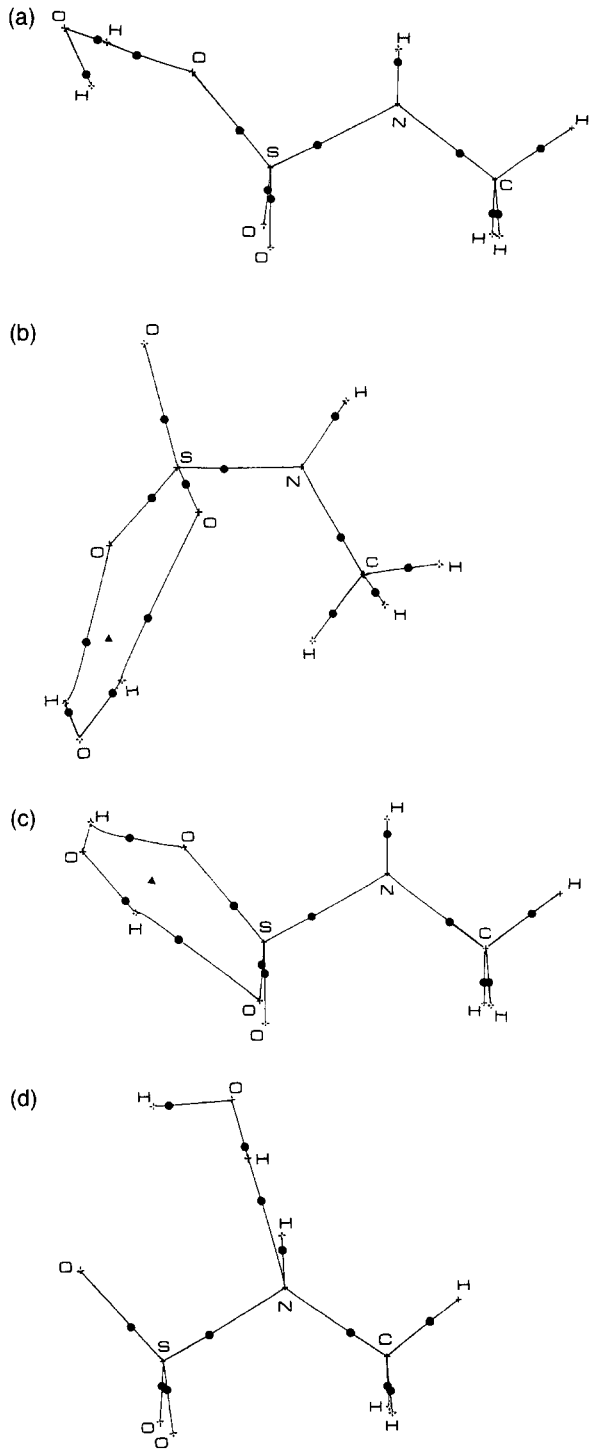

Fig. 6. Molecular graphs for four different water complexes of **1**. (a) Single H-bond to O_a. (b) Four-center H-bonds to O_{ga} and O_{gg}. Note the (3, +1) ring critical point. (c) Four center H-bonds to O_a and O_{gg}. Note the (3, +1) ring critical point. (d) Single H-bond to the N. All structures are optimized geometries from SCF 6-31+G** calculations. (3, −3) nuclear positions, +. (3, +1) RCPs, ▲, and (3, −1) BCPs, ●.

Table 5
Important optimized geometrical parameters of *N*-methyl sulfamate and water complexes **11a–d**

Complex	Bond lengths (Å)			
	11a	**11b**	**11c**	**11d**
C–N	1.4516	1.4519	1.4518	1.4550
N–S	1.6827	1.6803	1.6822	1.6984
N–H	1.0003	1.0001	1.0003	1.0022
S–O_a	1.4499	1.4532	1.4532	1.4469
S–O_{ga}	1.4520	1.4617	1.4518	1.4531
S–O_{gg}	1.4568	1.4450	1.4538	1.4504
$O_{gg} \cdots H_w$		2.1998	2.1937	
$O_a \cdots H_w$	1.9523		2.2117	
$O_{ga} \cdots H_{w'}$		2.1574		
$N \cdots H_w$				2.1199
$O_a \cdots O_w$	2.7076		3.0047	
$O_{ga} \cdots O_w$		2.9709		
$O_{gg} \cdots O_w$		2.9914	3.0115	
$N \cdots O_w$				3.0727
O_w–H_w	0.9553	0.9487	0.9487	0.9529
O_w–$H_{w'}$	0.9435	0.9495	0.9489	0.9529
	Bond angles (°)			
C–N–S	115.57	115.98	115.60	115.37
N–S–O_{gg}	104.64	104.46	104.38	103.74
N–S–O_{ga}	106.80	106.60	106.87	106.19
N–S–O_a	102.45	103.07	102.69	102.04
S–N–H	107.10	107.14	107.07	106.24
H_w–O_a–S	111.56			
O_a–H_w–O_w			142.79	
O_{ga}–$H_{w'}$–O_w		143.52		
O_{gg}–$H_{w'}$–O_w		140.25	141.35	
C–N–H_w				123.95
H_w–O–$H_{w'}$	103.33	101.10	101.08	103.13
	Torsion angles (°)			
N–S–O_{gg}–H_w	−109.74			
C–N–S–O_w		6.15	126.57	
N–S–O_w–H_w		92.11	−91.69	
N–S–O_w–$H_{w'}$		−93.65	89.59	
H–C–N–H_w				−55.57

developed molecular-modeling parameters by fitting force-field functions to experimental X-ray diffraction data [36]. We chose to develop parameters by fitting ab initio results. A data set was built up by systematic variation, using the adiabatic mapping algorithm, of the various bond lengths, bond angles and bond torsions. All force-field parameters were obtained by nonlinear least-squares fitting to this ab initio data set and are presented in Table 1.

Of particular interest are the torsion potential-energy curves. The ab initio curve for rotation about the S–N bond of *N*-methyl sulfamate is shown in Fig. 7a, and the ab

Table 6
Methyl sulfamate and water complexes **11a–d**: Selected topological properties of electron-density distributions at the BCPs and their hydrogen-bond energies in kcal mol^{-1} from 6-31+G** calculations [a]

Bond	ρ_b (au)	$\nabla^2\rho_b$ (au)	ϵ	H_b (Hartree Å^{-3})
11a C–N	0.2736	−0.8813	0.0193	−2.6739
11a N–S	0.2277	−0.1580	0.0574	−1.9602
11a S–O_a	0.2930	1.2796	0.0378	−2.2363
11a S–O_{ga}	0.2970	1.3382	0.0410	−2.2721
11a S–O_{gg}	0.2959	1.3231	0.0440	−2.2674
11a N–H	0.3603	−1.9623	0.0534	−3.7178
11a O_{gg}–H_w	0.0225	0.0748	0.0889	0.0027
11a O_w–H_w	0.3696	−2.5643	0.0224	−4.7947
11a O_w–$H_{w'}$	0.3909	−2.4355	0.0246	−4.6712
ΔE(**11a**) = −12.91 kcal mol^{-1}				
11b C–N	0.2729	−0.8708	0.0188	−2.6766
11b N–S	0.2285	−0.1481	0.0538	−1.9669
11b S–O_a	0.2995	1.3796	0.0336	−2.2930
11b S–O_{ga}	0.2948	1.3111	0.0405	−2.2512
11b S–O_{gg}	0.2907	1.2421	0.0473	−2.2228
11b N–H	0.3604	−1.9631	0.0541	3.7191
11b O_{ga}–H_w	0.0150	0.0504	0.0496	−0.0014
11b O_{gg}–H_w	0.0162	0.0530	0.0605	−0.0054
11b O_w–H_w	0.3817	−2.5179	0.0232	−4.7576
11b O_w–H_w	0.3803	−2.5251	0.0231	−4.7643
11b RCP [b]	0.0073	0.0040		
ΔE(**11b**) = −14.54 kcal mol^{-1}				
11c C–N	0.2733	−0.8776	0.0191	−2.6732
11c N–S	0.2280	−0.1572	0.0578	−1.9635
11c S–O_a	0.2946	1.3053	0.0367	−2.2492
11c S–O_{ga}	0.2949	1.3115	0.0406	−2.2519
11c S–O_{gg}	0.2961	1.3246	0.0442	−2.2687
11c N–H	0.3603	−1.9618	0.0535	−3.7178
11c O_{ga}–H_w	0.0145	0.0488	0.0479	−0.0014
11c O_a–H_w	0.0150	0.0498	0.0532	−0.0014
11c O_w–H_w	0.3816	−2.5191	0.0233	−4.7583
11c O_w–H_w	0.3812	−2.5219	0.0233	−4.7616
11c RCP [b]	0.0068	0.0376		
ΔE(**11c**) = −14.19 kcal mol^{-1}				
11d C–N	0.2711	−0.8578	0.0155	−2.6515
11d N–S	0.2209	−0.1948	0.0439	−1.8839
11d S–O_a	0.2966	1.3335	0.0393	−2.2674
11d S–O_{ga}	0.2983	1.3695	0.0441	−2.2795
11d S–O_{gg}	0.2953	1.3129	0.0474	−2.2606
11d N–H	0.3595	−1.9551	0.0483	−3.7043
11d N–H_w	0.0198	0.0550	0.0337	−0.0007
11d O_w–H_w	0.3738	−2.5460	0.0231	−4.7819
11d O_w–H_w	0.3894	−2.4543	0.0244	−4.6894
ΔE(**11d**) = −11.54 kcal mol^{-1}				

[a] H_2O E(SCF) = −76.03123306 au at the same level of theory.
[b] Actually these are ρ_r and $\nabla^2\rho_r$.

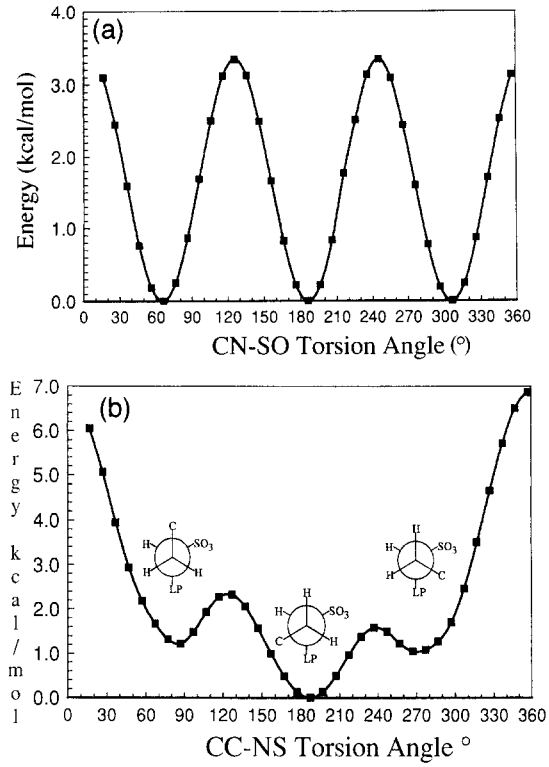

Fig. 7. Gas-phase (0 K) torsion potentials for rotations about (a) the CN–SO_a bond in **1** and (b) the CC–NS bond in **2**. All energies from SCF 6-31+G** calculations.

initio curve for the N–C bond of *N*-ethyl sulfamate is shown in Fig. 7b. For the S–N bond the usual three-parameter Fourier analysis fits well, but for the N–C bond some discrepancy is found since the ab initio curve is not symmetric. The MM+ calculated torsion potential (not shown) for the C–N bond of *N*-methyl sulfamate anion is superimposable on the curve in Fig. 7a. The corresponding MM+ calculated curve for the N–C bond is also almost superimposable between 70° and 210°. For eclipsing conformations strong van der Waals repulsions create energy barriers that are too high. The torsional portion of the energy barrier fits the ab initio data well (not shown).

Successful modeling of the charged functional groups requires careful attention to electrostatics [35]. The present version of MM+ (see Experimental) allows for the use of point charges to estimate electrostatic interactions. Due to the strong $1/r$ dependence, these terms are usually dominant in the molecular modeling. Table 7 gives the atomic charges calculated by the Bader AIM method, by the AM1 semiempirical method, and those from the ab initio calculations (see Experimental for details of calculations). The AIM method is conceptually different from the other methods (for a discussion see ref. [37]). Also shown for comparison are the calculated charges for *O*-methyl **5** and ethyl sulfate **6**. The large positive charges on sulfur and the smaller but still large negative

Table 7
Selected ab initio and AM1 (Mulliken) point charges as well as Bader's AIM atomic charges for *O*-methyl sulfate **5**, *N*-methyl sulfamate **1**, ethyl sulfate **6** and *N*-ethyl sulfamate **2** anions

Atom	*O*-Methyl sulfate **5**	*N*-Methyl sulfamate **1**	**1** AM1	**1** Bader's AIM
C	−0.142	−0.2758	−0.0814	0.6723
N	−0.7041(O)	−0.7485	−0.8216	−1.4872
HC	0.0907	0.0873	0.0395	−0.0987
HC	0.1289	0.1249	0.0492	−0.0662
HC	0.1289	0.1459	0.0905	−0.0317
S	2.2353	2.0824	2.7287	4.3039
O_a	−0.8864	−0.9083	−1.0490	−1.4872
O_{ga}	−0.9257	−0.9194	−1.0471	−1.5597
O_{gg}	−0.9257	−0.8944	−1.0761	−1.5658
HN	–	0.3059	0.1673	0.3906
	Ethyl sulfate **6**	*N*-ethyl sulfamate **2**	**2** AM1	**2** Bader's AIM
C-1	−0.4524	−0.4026	−0.2283	0.2220
C-2	0.0303	−0.1571	−0.1709	0.6441
HC-2	0.1288	0.1030	0.0514	−0.0993
HC-2	0.1284	0.1463	0.0932	−0.0363
HC-2	0.1284	0.1241	0.02465	−0.0758
N	−0.7509(O)	−0.7780	−0.8890	−1.4961
HC-1	0.1028	0.1048	0.04909	−0.1015
HC-1	0.1288	0.1347	0.0762	−0.0685
S	2.2761	2.1160	2.8371	4.3066
O_a	−0.8808	−0.8978	−1.0745	−1.5600
O_{ga}	−0.9198	−0.9165	−1.0748	−1.5599
O_{gg}	−0.9197	−0.8827	−1.0731	−1.5658
HN	–	0.3057	0.1910	0.3880

values on nitrogen and oxygen reflect the highly polarized nature of these bonds. The ab initio Mulliken charges led to satisfactory structures (RMSD for **1**, 0.1599 and for **2**, 0.1528, see below). However, we have chosen to use the AM1 values for these molecular studies since it is just feasible to calculate these charges for the large systems (**8**–**10**) modeled below. We include the other values since readers may find them useful for their applications.

Little experimental data is available with which to compare the MM+ calculated results. We have used our ab initio results for **1** and **2** and the 4-31 + G** literature results for *N*-isopropyl sulfamate **7** [29]. In the last case, two conformers were found that differed in energy by 0.54 kcal mol^{-1}. The third staggered conformer with both methyls *gauche* to the nitrogen was found to be 5.02 kcal mol^{-1} higher in energy (see Fig. 8 for structures of **7**). The conformational spaces were sampled using the torsion-angle-searching algorithm of ref. [16], implemented in Hyperchem v. 4 [38]. The RMSD for all atoms for **1** searched using this algorithm was 0.1149 and O_a–S–N–C = −179.8°. For **2** the lowest-energy conformer has an RMSD of 0.0764, S–N–C–C = −179.3°. Two other conformers with S–N–C–C = 93.3° and −93.7° and 1.10 and 1.31 kcal mol^{-1} above the minimum were also found. For **7** three conformers with S–N–C–H torsion

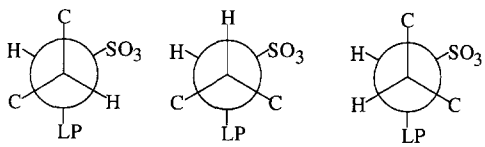

Fig. 8. Newman projections about the C–N bond of *N*-isopropylsulfamate **7** showing the three staggered rotamers.

Table 8
Comparison of gas-phase calculated structures with X-ray structures of 2-deoxy-2-sulfoamino-α-D-glucose salt derivatives (**8–10**)

		Bond lengths (Å)					
		C–N	N–S	S–O_a	S–O_{ga}	S–O_{gg}	N–H
8	Experimental	1.503	1.639	1.466	1.457	1.447	1.01 [a]
	Calculated	1.485	1.687	1.476	1.486	1.462	1.001
9	Experimental	1.446	1.641	1.453	1.474	1.441	[a]
	Calculated	1.493	1.680	1.452	1.441	1.468	0.998
10	Experimental	1.442	1.629	1.451	1.472	1.450	[a]
	Calculated	1.477	1.663	1.465	1.440	1.443	1.003
		Bond angles (°)					
		C–N–S	N–S–O_a	N–S–O_{ga}	N–S–O_{gg}	O_a–S–O_{ga}	
8	Experimental	118.01	102.09	105.92	111.33	113.36	
	Calculated	122.62	102.87	106.29	106.07	113.33	
9	Experimental	117.74	100.35	109.79	106.49	111.55	
	Calculated	121.78	100.34	104.24	106.24	117.59	
10	Experimental	119.64	103.09	109.98	105.37	112.01	
	Calculated	122.92	92.17	102.93	104.81	117.61	
		O_a–S–O_{gg}	O_{ga}–S–O_{gg}	S–N–H	C–N–H		
8	Experimental	111.60	111.97	109.47 [a]	109.47 [a]		
	Calculated	114.48	112.70	97.34	107.96		
9	Experimental	114.48	110.74	[a]	[a]		
	Calculated	112.81	113.57	98.87	112.26		
10	Experimental	111.94	110.86	[a]	[a]		
	Calculated	116.19	117.30	96.39	100.70		
		Bond torsions (°)					
		C_2–N–S–O_a	C_1–C_2–N–S	C_2–C_3–O–S			
8	Experimental	−170.57	110.66	n.a.			
	Calculated	−172.47	111.34				
9	Experimental	168.93	104.06	−105.87			
	Calculated	165.20	132.80	114.26			
10	Experimental	171.97	98.71	−99.32			
	Calculated	176.82	64.80	−117.12			

[a] Default values.

angles of −41.3°, 36.7°, and 172.7°, and relative energies of 0, 1.00, and 4.10 kcal mol^{-1} were found in substantial agreement with the 4-31 + G** ab initio results.

We have also used the X-ray diffraction results for 2-deoxy-2-sulfoamino-α-D-glucose dihydrate, sodium salt (**8**) [39], 2-deoxy-3-*O*-sulfo-2-sulfoamino-α-D-glucose trihydrate, disodium salt (**9**), and methyl 2-deoxy-3-*O*-sulfo-2-sulfoamino-α-D-glucosamine tetrahydrate, disodium salt (**10**) [40]. The hydrogen atoms were not accurately found in the solid-state structures and were thus added in the standard geometries. In all cases the MM+ calculations adequately reproduced the N–S and O–S bond lengths and associated bond angles. The RMSDs for all atoms, except the hydroxyl hydrogens and counter-ions or waters of hydration, are 0.3546 in **8**, 0.5872 in **9**, and 0.6784 in **10**. For salts **8–10** the experimental C-2–N–S–O_a torsion angle is 176.8 ± 6.39°, in excellent agreement with the calculated value of 174.9 ± 11.45°. However, the experimental S–N–C-2–C-1 torsion angle is 104.48 ± 5.99°, whereas the lowest-energy conformer found from searching this angle was 72.3 ± 2.0 for **8–10**. Both the experimental values and the MM+ calculated ones are in one of the secondary ab initio minima of Fig. 7b, but the corresponding angle for S–N–C-2–C-3 is 224.6°, which is not in an ab initio minimum for **2**. The MM+ calculated value for S–N–C-2–C-3 is 192.4°, which is in the main ab initio minimum. In the absence of compensating steric or electrostatic interactions, the MM+ calculated torsion is determined by the potential fit to the curve for **2**. This result suggests that the solid-state S–N–C-2(C) torsions are at least partly determined by such steric or electrostatic interactions such as intermolecular contacts not modeled in these calculations.

Preliminary MM+ calculations incorporating the sodium cation (see Experimental) led to improved results for this torsion angle with average values 102.98 ± 34.76°. These geometries are tabulated in Table 8. Ferro et al. [35] have modified their version of the MM program to reproduce the crystal packing of several alkali cation salts of sulfates [41] and **8**. The use of their parameters could improve the fits reported here. The starting coordinates for the sodium cation were found to be very important. For example, three complexes with the sodium cation complexed to each of the three terminal oxygens of the *N*-sulfo group were found that differed in energy as follows: O_a, 0.00; O_{gg}, 0.91; and O_{gu}, 2.01 kcal mol^{-1}. No bidentate complexes were found.

4. Conclusions

Heparin is known to have both specific and nonspecific interactions with proteins [42]. For example, heparin interacts nonspecifically with thrombin but specifically with antithrombin [9]. The latter interaction is mediated by a specific pentasaccharide sequence [43]. Numerous derivatives of this pentasaccharide have been prepared and tested. One of the more remarkable results is the exchange of one sulfate for a phosphate, which results in almost complete loss of biological activity [44]. This result suggests that a highly specific sulfate interaction should exist in the heparin–antithrombin complex, but no explanation for this result is at present known. Other derivatives replaced the sulfamates with sulfates with retained activity [45]. Since this modification greatly reduces the synthetic complexity, it leads to potentially useful mimetics [46].

The heparin binding site of antithrombin has been partly elucidated by molecular modeling [33] and is proposed to involve a complementary array of Arg and Lys side chains. Other heparin-binding proteins have been proposed to form "cationic cradles" by bringing together basic amino acids from discontinuous portions of the polypeptide chain [47]. The strong ionic strength dependence of thermodynamic properties of heparin–protein binding also clearly indicate the importance of electrostatic interactions. In one example, the binding of heparin to mucus proteinase inhibitor is characterized by five to six sites, each contributing about 2.5 kcal mol^{-1} towards the binding enthalpy.

None of these studies distinguish between the nondirectional Model A and the directional Model B for ion-pair formation of Fig. 2. The direct involvement of hydrogen-bonding to sulfate anions has been shown in a few model studies. For example, a calixarene tetrasulfonamide-amide binds HSO_4^- selectively [48]. A polycyclic quinoline phenol derivative forms hydrogen-bond stabilized ion-pairs with *p*-toluenesulfonic acid [49]. Finally a series of lipophilic bis-guanidinium compounds

Table 9
Intra- and inter-molecular contacts (< 3.2 Å) of the *N*- and *O*-sulfo groups [a] (distances in Å)

2-Deoxy-2-sulfoamino-α-D-glucose dihydrate, sodium salt (**8**)			
N(I) · · · O6(I + a)	3.109(9)	O2S(I) · · · OW2(III-b-2c)	3.019(9)
O_aS1(I) · · · OW1(I + a)	2.672(9)	O3S(I) · · · N(IV-b-2c)	3.015(8)
O_aS1(I) · · · O3(IV-b-2c)	2.787(7)	O3S(I) · · · O4(IV-a-b-2c)	2.758(8)
O2S(I) · · · Na(I)	2.382(7)		
2-Deoxy-3-*O*-sulfo-2-sulfoamino-α-D-glucose trihydrate, disodium salt (**9**)			
N(I) · · · O3W(IV-a-b-c)	2.996(16)	O_{ga}S1(I) · · · O4(I + a)	2.807(15)
O_aS1(I) · · · Na1(IV-a-b-c)	2.413(11)	O_{ga}S1(I) · · · O2W(IV-b-c)	2.955(17)
O_aS1(I) · · · Na2(IV-b-c)	2.359(12)	O_aS2(I) · · · Na2(IV-a-b-c)	2.421(11)
O_aS1(I) · · · O1W(IV-a-b-c)	3.152(13)	O_aS2(I) · · · O2W(IV-a-b-c)	2.957(15)
O_aS1(I) · · · O2W(IV-b-c)	3.215(16)	O_aS2(I) · · · O3W(IV-a-b-c)	3.244(14)
O_{gg}S1(I) · · · Na2(I)	2.524(11)	O_gS2(I) · · · Na2(I)	2.350(11)
O_{gg}S1(I) · · · O4(I + a)	3.187(15)	O_gS2(I) · · · Na1(IV-a-b-c)	2.411(11)
O_{gg}S1(I) · · · Na1(I + a)	2.478(12)	$O_{g'}$S2(I) · · · Na1(I)	2.448(11)
O_{gg}S1(I) · · · O1W(IV-a-b-c)	3.090(13)	$O_{g'}$S2(I) · · · O3W(I)	2.845(14)
O_{ga}S1(I) · · · O1(III-b-c)	2.845(13)	$O_{g'}$S2(I) · · · O1W(IV-2a-b-c)	2.888(14)
Methyl 2-deoxy-3-*O*-sulfo-2-sulfoamino-α-D-glucosamine tetrahydrate, disodium salt (**10**)			
N(I) · · · O3W(I)	3.041(4)	O_{ga}S1(I) · · · O2W(I + a)	2.911(4)
O_aS1(I) · · · Na1(IV-c)	2.383(2)	O_aS2(I) · · · Na2(I)	2.365(2)
O_aS1(I) · · · Na2(I + a)	2.322(2)	O_aS2(I) · · · O2W(I)	3.097(4)
O_aS1(I) · · · O1W(IV-b-c)	3.156(3)	O_gS2(I) · · · Na1(IV-c)	2.428(2)
O_{gg}S1(I) · · · O4(I + a)	3.159(3)	O_gS2(I) · · · Na2(IV-b-c)	2.366(2)
O_{gg}S1(I) · · · Na1(I + a)	2.454(2)	O_gS2(I) · · · O1W(IV-b-c)	3.216(3)
O_{gg}S1(I) · · · Na2(IV-b-c)	2.538(3)	$O_{g'}$S2(I) · · · Na1(I)	2.508(3)
O_{gg}S1(I) · · · O1W(IV-b-c)	3.060(3)	$O_{g'}$S2(I) · · · O1W(IV-a-b-c)	2.877(3)
O_{ga}S1(I) · · · O4(I + a)	2.743(3)	$O_{g'}$S2(I) · · · O3W(IV-b-c)	2.875(4)

[a] Explanation of nomenclature. Symmetry code: (I) = x, y, z; (II) = $-x+1/2, -y, z+1/2$; (III) = $x+1/2, -y+1/2, -z$; (IV) = $-x, y+1/2, -z+1/2$. Note all crystals are orthorhombic and belong to the space group $P2_12_12_1$. Cell parameters are $a = 7.713(1)$, $b = 9.390(2)$, $c = 17.222(2)$ for **8**; $a = 7.883(1)$, $b = 8.953(1)$, $c = 22.391(2)$ for **9**; $a = 7.818(1)$, $b = 8.996$ (1), $c = 26.734(5)$ for **10**.

selectively extract SO_4^- anions into chloroform [50]. Perhaps the most relevant example is the existence of an intermolecular bifurcated hydrogen-bonding system in the crystal lattice of **8**. In this case the sulfamate hydrogen ($N \cdots O_{gg}$, 3.015 Å) and the O-3 hydrogen ($O \cdots O_a$, 2.787 Å) of one sugar residue act as donors, and two sulfamate S = O oxygens of another residue act as acceptors. These bond lengths ($O_w \cdots O$, 2.97 and 2.99 Å in **11b** and 3.01 and 3.01 Å in **11c**, see Table 5) resemble those found in the calculated water complexes. Table 9 includes a complete set of the experimental short-distance contacts to the sulfate groups in **8–10**. All sulfate oxygens form short contacts. Since the hydrogens were not accurately located, the nature of the hydrogen-bonding interactions is not precise, but most are based on distance and angle constraints for single hydrogen bonds like **11a**. It also appears that the sulfoamino hydrogen can act as hydrogen-bond donor. Together these experimental and theoretical results suggest that, at least in some cases, specific directional hydrogen-bonded structures like Model B in Fig. 2 probably exist in protein–heparin complexes. Such types of binding interactions provide a mechanism for selectivity.

Acknowledgements

The continuing financial support of the Natural Sciences and Engineering Research Council (NSERC) of Canada is gratefully acknowledged. This is NRC paper no. 39506.

References

[1] L. Rodén, in D.A. Lane and U. Lindahl (Eds.), *Heparin — Chemical and Biological Properties*, CRC Press, Boca Raton, FL, 1989, pp 1–24.
[2] (a) J. Riesenfeld, L. Thunberg, M. Höök, and U. Lindahl, *J. Biol. Chem.*, 256 (1981) 2389–2394; (b) D.H. Atha, J.C. Lormeau, M. Petitou, R.D. Rosenberg, and J. Choay, *Biochemistry*, 24 (1985) 6723–6729.
[3] (a) D.J. Tyrrell, M. Ishihara, N. Rao, A. Horne, M.C. Kiefer, G.B. Stauber, L.H. Lam, and R.J. Stack, *J. Biol. Chem.*, 268 (1993) 4684–4689; (b) M. Maccarana, B. Casu, and U. Lindahl, *J. Biol. Chem.*, 268 (1993) 23898–23905.
[4] B.C. Herold, S.I. Gerber, T. Polonsky, B.J. Belval, P.N. Shaklee, and K. Holme, *Virology*, 206 (1995) 1108–1116.
[5] (a) Y. Yamaguchi, *Trends Glycosci. Glycotechnol.*, 5 (1993) 428–437; (b) R.L. Jackson, S.J. Busch, and A.D. Cardin, *Physiol. Rev.*, 71 (1991) 481–539; (c) M. Witvrouw, J. Desmyter, and E. De Clercq, *Antiviral Chem. Chemother.*, 5 (1994) 345–359.
[6] D.M. Whitfield and T.-H. Tang, *J. Am. Chem. Soc.*, 115 (1993) 9648–9654.
[7] D.A. Forsyth and S.M. Johnson, *J. Am. Chem. Soc.*, 116 (1994) 11481–11484.
[8] C. Chang and R.F.W. Bader, *J. Phys. Chem.*, 96 (1992) 1654–1662.
[9] S.T. Olson and I. Björk, *Semin. Thromb. Hemostas.*, 20 (1994) 373–409.
[10] B. Lomonte, E. Moreno, A. Tarkowski, L.A. Hanson, and M. Maccarana, *J. Biol. Chem.*, 269 (1994) 29867–29873.
[11] M. Ishihara, *Glycobiology*, 4 (1994) 817–824.
[12] (a) L.D. Thompson, M.W. Pantoliano, and B.A. Springer, *Biochemistry*, 33 (1994) 3831–3840; (b) J. Bae, U.R. Desai, A. Pervin, E.E.O. Caldwell, J.M. Weiler, and R.J. Linhardt, *Biochem. J.*, 301 (1994) 121–129; (c) S.A. Thompson, S. Higashiyama, K. Wood, N.S. Pollitt, D. Damm, G. McEnroe, B. Garrick, N. Ashton, K. Lau, N. Hancock, M. Klagsbrun, and J.A. Abraham, *J. Biol. Chem.*, 269 (1994) 2541–2549; (d) A. Horne and P. Gettins, *Biochemistry*, 31 (1992) 2286–2294.

[13] (a) D.S. Ferran, M. Sobel, and R.B. Harris, *Biochemistry*, 31 (1992) 5010–5016; (b) H. Margalit, N. Fischer, and S.A. Ben-Sasson, *J. Biol. Chem.*, 268 (1993) 19228–19231.
[14] D.L. Rabenstein, P. Bratt, T.D. Schierling, J.M. Robert, and W. Guo, *J. Am. Chem. Soc.*, 114 (1992) 3278–3285.
[15] (a) N.L. Allinger, *J. Am. Chem. Soc.*, 99 (1977) 8127–8134; (b) U. Burkert and N.L. Allinger, *Molecular Mechanics*, American Chemical Society, Washington, DC, 1982; (c) N.L. Allinger, Y.H. Yuh, and J.-H. Lii, *J. Am. Chem. Soc.*, 111 (1989) 8551–8566.
[16] I. Kolossváry and W.C. Guida, *J. Comput. Chem.*, 14 (1993) 691–698.
[17] (a) M.J.S. Dewar, *J. Am. Chem. Soc.*, 108 (1986) 8075–8086; (b) M.J.S. Dewar and Y.-C. Yuan, *Inorg. Chem.*, 29 (1990) 3881–3890.
[18] N.L. Allinger and Y. Fan, *J. Comput. Chem.*, 14 (1993) 655–666.
[19] M.J. Frisch, M. Head-Gordon, H.B. Schlegel, K. Raghavachari, J.S. Binkley, C. Gonzalez, D.J. Defrees, D.J. Fox, R.A. Whiteside, R. Seeger, C.F. Melius, J. Baker, R.L. Martin, L.R. Kahn, J.J.P. Stewart, E.M. Fluder, S. Topiol, and J.A. Pople, *GAUSSIAN 88*, Gaussian, Inc., Pittsburgh, PA, 1988.
[20] M.J. Frisch, G.W. Trucks, M. Head-Gordon, P.M.W. Gill, M.W. Wong, J.B. Foresman, B.G. Johnson, H.B. Schlegel, M.A. Robb, E.S. Replogle, R. Gomperts, J.L. Andres, K. Raghavachari, J.S. Binkley, C. Gonzalez, R.L. Martin, D.J. Fox, D.J. Defrees, J. Baker, J.J.P. Stewart, and J.A. Pople, *GAUSSIAN 92*, Revision C, Gaussian, Inc., Pittsburgh, PA, 1992.
[21] W.J. Hehre, R. Ditchfield, and J.A. Pople, *J. Chem. Phys.*, 56 (1972) 2257–2261.
[22] R.S. Mulliken, *J. Chem. Phys.*, 36 (1962) 3428–3432.
[23] (a) R.F.W. Bader, *Chem. Rev.*, 91 (1991) 893–928; (b) R.F.W. Bader, *Atoms in Molecules: A Quantum Theory*, Clarendon Press, Oxford, 1990; (c) R.F.W. Bader, *Acc. Chem. Res.*, 18 (1985) 9–15.
[24] T.-H. Tang, D.M. Whitfield, S.P. Douglas, J.J. Krepinsky, and I.G. Csizmadia, *Can. J. Chem.*, 72 (1994) 1803–1825.
[25] (a) D. Cremer and E. Kraka, *Croat. Chim. Acta*, 57 (1984) 1259–1281; (b) E. Kraka and D. Cremer, in Z.B. Makisc (Ed.), *Theoretical Models of Chemical Bonding*, Part 2, Springer, Berlin, 1990, p 452.
[26] F.W. Biegler-König, R.F.W. Bader, and T.-H. Tang, *J. Comput. Chem.*, 3 (1982) 317–326.
[27] R.J. Gillespie and I. Hargittai, *The VSEPR Model of Molecular Geometry*, Prentice Hall, London, 1991.
[28] M.W. Wong, K.B. Wiberg, and M.J. Frisch, *J. Am. Chem. Soc.*, 114 (1992) 523–529.
[29] C.J.M. Huige and C. Altona, *J. Comput. Chem.*, 16 (1995) 56–79.
[30] R.D. Bindal, J.T. Golab, and J.A. Katzenellenbogen, *J. Am. Chem. Soc.*, 112 (1990) 7861–7868.
[31] G.A. Jeffrey, H. Maluszynska, and J. Mitra, *Int. J. Biol. Macromol.*, 7 (1985) 336–348.
[32] (a) A.D. Cardin and H.J.R. Weintraub, *Arteriosclerosis*, 9 (1989) 21–32; (b) D.R. Ferro, A. Provasoli, M. Ragazzi, G. Torri, B. Casu, G. Gatti, J.C. Jacquinet, P. Sinaÿ, M. Petitou, and J. Choay, *J. Am. Chem. Soc.*, 108 (1986) 6773–6778.
[33] P.D.J. Grootenhuis and C.A.A. van Boeckel, *J. Am. Chem. Soc.*, 113 (1991) 2743–2747.
[34] (a) M. Ragazzi, D.R. Ferro, and A. Provasoli, *J. Comput. Chem.*, 7 (1986) 105–112; (b) P. Kaliannan, S. Vishveshwara, and V.S.R. Rao, *J. Mol. Struct.*, 105 (1983) 359–374; (c) J.M. Park, O.Y. Kwon, K.T. No, M.S. Jhon, and H.A. Scheraga, *J. Comput. Chem.*, 16 (1995) 1011–1026.
[35] D.R. Ferro, P. Pumilia, A. Cassinari, and M. Ragazzi, *Int. J. Biol. Macromol.*, 17 (1995) 131–136.
[36] J.Y. Le Queste, S. Cros, W. Mackie, and S. Pérez, *Int. J. Biol. Macromol.*, 17 (1995) 161–175.
[37] K.B. Wiberg and P.R. Rablen, *J. Comput. Chem.*, 14 (1993) 1504–1518.
[38] C.E. Peishoff and J.S. Dixon, *J. Comput. Chem.*, 13, (1992) 565–569.
[39] (a) E.A. Yates, W. Mackie, and D. Lamba, *Int. J. Biol. Macromol.*, 17 (1995) 219–226; (b) W.H. Ojala, K.E. Albers, W.B. Gleason, and C.C. Choo, *Carbohydr. Res.*, 275 (1995) 49–65; (c) W. Mackie, E.A. Yates, and D. Lamba, *Carbohydr. Res.*, 266 (1995) 65–74.
[40] D. Lamba, unpublished data.
[41] D. Lamba, S. Glover, W. Mackie, A. Rashid, B. Sheldrick, and S. Pérez, *Glycobiology*, 4 (1994) 151–163.
[42] D.P. Mascotti and T.M. Lohman, *Biochemistry*, 34 (1995) 2908–2915.
[43] C.A.A. von Boeckel and M. Petitou, *Angew. Chem., Int. Ed. Engl.*, 32 (1993) 1671–1690.
[44] J.N. Vos, P. Westerduin, and C.A.A. van Boeckel, *Bioorg. Med. Chem. Lett.*, 1 (1991) 143–146.
[45] J. Basten, G. Jaurand, B. Olde-Hanter, P. Duchaussoy, M. Petitou, and C.A.A. van Boeckel, *Bioorg. Chem. Med. Lett.*, 2 (1992) 905–910.

[46] M. Petitou and C.A.A. van Boeckel, in W. Her, G.W. Kirby, and C.H. Tamm (Eds.), *Progress in the Chemistry of Natural Products*, Springer, Berlin, 1992, pp 144–210.
[47] (a) D.M. Mann, E. Romm, and M. Migliorini, *J. Biol. Chem.*, 269 (1994) 23661–23667; (b) T.F. Busby, W.S. Argraves, S.A. Brew, I. Pechik, G.L. Gilliland, and K.C. Ingham, *J. Biol. Chem.*, 270 (1995) 18558–18562; (c) Y.G. Brickman, M.D. Ford, D.H. Small, P.F. Bartlett, and V. Nurcombe, *J. Biol. Chem.*, 270 (1995) 24941–24948.
[48] Y. Morzherin, D.M. Rudkevich, W. Verboom, and D.N. Reinhoudt, *J. Org. Chem.*, 58 (1993) 7602–7605.
[49] K. Manabe, K. Okamura, T. Date, and K. Koga, *J. Org. Chem.*, 58 (1993) 6692–6700.
[50] H. Stephan, K. Gloe, P. Schiessl, and F.P. Schmidtchen, *Supramol. Chem.*, 5 (1995) 273–280.